Impedance Control of an aerial-manipulator: Preliminary results

E. Cataldi[1], G. Muscio[2], M. A. Trujillo[3],Y. Rodriguez[3], F. Pierri[2], G. Antonelli[1], F. Caccavale[2], A. Viguria[3], S. Chiaverini[1] and A. Ollero[4]

***Abstract*— In this paper, an impedance control scheme for aerial robotic manipulators is proposed, with the aim of reducing the end-effector interaction forces with the environment. The proposed control has a multi-level architecture, in detail the outer loop is composed by a trajectory generator and an impedance filter that modifies the trajectory to achieve a complaint behaviour in the end-effector space; a middle loop is used to generate the joint space variables through an inverse kinematic algorithm; finally the inner loop is aimed at ensuring the motion tracking. The proposed control architecture has been experimentally tested.**

I. Introduction

Over the last years, the development of technologies of Unmanned Aerial Vehicles (UAVs) coincides with the increasing of applications where, requiring not only autonomous flight but also interaction with the environment. An emerging application is the aerial manipulation: UAVs equipped with grippers have been proposed in literature, as in [1] or in [2], where a compliant gripper with four fingers is adopted.

More recently, developments in light-weight robotic arms allow the adoption of multi-degree of freedoms (DOFs) manipulators mounted on UAV platforms, as in [3], where a UAV with a 3-arm manipulator, with 2 DOFs for each arm, is proposed; in [4], a 5-DOFs robotic arm is adopted and the aerial manipulator is controlled through a hierarchical control scheme, while in [5] and [6], experiments on a UAV with a 6-DOFs manipulator are described.

Aerial manipulators have been used in operations involving the interaction with the external environment, such as in [7], where the authors presented experiments on a quadrotor equipped with two 2-DoFs arms turning a valve. Similar experiments have been presented at 2015 ICRA conference: in [8] the authors proposed a new configuration of an aerial manipulator able to accomplish knob-twisting and door-pushing operations; in [9] an aerial manipulator is adopted for opening and closing a drawer.

To cope with external environment interactions, the impedance control [10] is a well established strategy for ground-fixed manipulators. In the last years, it has been successfully extended to aerial manipulation: the authors in [11] proposed a Cartesian impedance control law, aimed at counteracting both external contact forces and external disturbances, while in [12] a selective compliant behavior is imposed to the manipulator end-effector interacting with the environment. In [13] the system composed by two aerial manipulators grasping a common object is considered: two impedance laws are proposed to confer a compliant behavior to the object (external impedance) and avoid large internal stresses (internal impedance). In [14] the detailed model of a ducted-fan aerial vehicle with a robotic manipulator is presented and the impedance control paradigm is adopted to handle contacts with the environment.

In this paper, an admittance control for aerial manipulators, based on a multi-layer architecture, is proposed in order to handle the generalized forces acting on the manipulator wrist due to the interaction with the environment. The highest level includes an impedance filter, that receives from an off-line planner the desired trajectory for the end-effector and, on the basis of the measured forces coming from a wrist-mounted force/torque sensor, outputs a new reference trajectory, designed to reduce the contact forces. The middle level is an inverse kinematics module, that, based on the output of the previous layer, generates the reference values for the motion variables (position and attitude of the vehicle and joint position). The lowest layer is a dynamic motion controller in charge of tracking the references output by the upper layer. The effectiveness of the approach is proven via an experimental campaign (see Fig. 1) performed on a multirotor vehicle with a 6-DOFs manipulator, available at the CATEC (Centro Avanzado de Tecnologas Aeroespaciales) institute in Sevilla. Such experimental setup has been designed and developed within the EU-funded ARCAS (Aerial Robotics Cooperative Assembly System) project [15], aimed at developing a cooperative free-flying robot system for assembly and structure construction.

II. Modeling

Let us consider an aerial manipulation system composed by an Unmanned Aerial quadrotor Vehicle and a n-DOFs robotic Manipulator (UAVM), with all revolute joints (Fig. 1). The quadrotor is an under-actuated system with four input forces and six DOFs then only four of its DOFs are controllable, describing position and orientation of its center of mass. Therefore, the whole system is characterized by $4+n$ DOFs, where n is the number of DOFs of the arm.

[1] G. Antonelli, E. Cataldi and S. Chiaverini are with University of Cassino and Southern Lazio, Cassino, Italy. Corresponding author: Elisabetta Cataldi, e-mail: e.cataldi@unicas.it.

[2] F. Caccavale, G. Muscio and F. Pierri are with University of Basilicata, Potenza, Italy.

[3] M.A. Trujillo and A. Vigura are with Center for Advanced Aerospace Technologies (CATEC), Sevilla, Spain.

[4] A. Ollero is with University of Sevilla, Sevilla, Spain.

Preprint version of the paper: E. Cataldi, G. Muscio, M.A. Trujillo, Y. Rodriguez, F. Pierri, G. Antonelli, F. Caccavale, A. Viguria, S. Chiaverini, A. Ollero, "Impedance control of an aerial-manipulator: Preliminary results" IEEE/RSJ International Conference on Intelligent Robots and Systems, pp. 3848-3853, 2016. DOI:10.1109/IROS.2016.7759566

Fig. 1. The aerial manipulator during the experiments, involving interaction with a rope (left) and a semi-flexible bar (right).

A. Kinematics

Let Σ_e be the reference frame attached to the end-effector, Σ_b the reference frame with origin at the vehicle's center of mass and Σ the inertial reference frame (see Fig. 2).

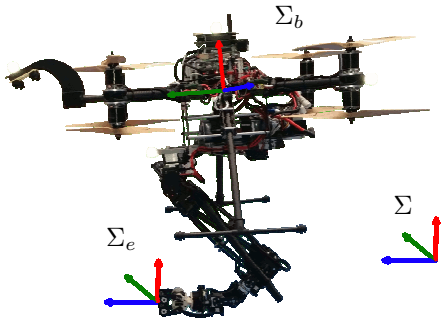

Fig. 2. The aerial manipulator with the defined reference frames: Σ (inertial reference frame), Σ_b (vehicle body reference frame) and Σ_e (end-effector reference frame).

The end-effector position, $\boldsymbol{p}_e$, and orientation, expressed in terms of Euler angles (RPY), $\boldsymbol{\phi}_e = [\varphi_e, \theta_e, \psi_e]^{\mathrm{T}}$, are given by the following equations

$$\boldsymbol{p}_e = \boldsymbol{p}_b + \boldsymbol{R}_b \boldsymbol{p}^b_{e_b}, \tag{1}$$
$$\boldsymbol{\phi}_e = \boldsymbol{\phi}(\boldsymbol{R}_b \boldsymbol{R}^b_e), \tag{2}$$

where $\boldsymbol{p}^b_{e_b}$ and $\boldsymbol{R}^b_e$ denote the position and orientation of Σ_e with respect to Σ_b, $\boldsymbol{p}_b$ and $\boldsymbol{R}_b$ represent the position and orientation of the vehicle with respect to Σ, while $\boldsymbol{\phi}(\boldsymbol{R}_b \boldsymbol{R}^b_e)$ denotes the RPY angles extracted from the rotation matrix $\boldsymbol{R}_b \boldsymbol{R}^b_e$. The linear velocity, $\dot{\boldsymbol{p}}_e$, and angular velocity, $\boldsymbol{\omega}_e$, of the end-effector, obtained by differentiating (1) and the rotation matrix $\boldsymbol{R}_b \boldsymbol{R}^b_e$, are computed as follows

$$\dot{\boldsymbol{p}}_e = \dot{\boldsymbol{p}}_b - \boldsymbol{S}(\boldsymbol{R}_b \boldsymbol{p}^b_{e_b}) \boldsymbol{\omega}_b + \boldsymbol{R}_b \dot{\boldsymbol{p}}^b_{e_b}, \tag{3}$$
$$\boldsymbol{\omega}_e = \boldsymbol{\omega}_b + \boldsymbol{R}_b \boldsymbol{\omega}^b_e, \tag{4}$$

where $\boldsymbol{\omega}_b$ and $\boldsymbol{\omega}^b_e$ are the angular velocity of Σ_b with respect to the inertial reference and the angular velocity of Σ_e relative to Σ_b, respectively, while $\boldsymbol{S}(\cdot)$ is the (3×3) skew-symmetric matrix operator performing the cross product [16]. By exploiting the transformation matrix $\boldsymbol{T}(\cdot)$ relating the angular velocity and the Euler angles rate [16], (3) and (4) can be rewritten as

$$\dot{\boldsymbol{p}}_e = \dot{\boldsymbol{p}}_b - \boldsymbol{S}(\boldsymbol{R}_b \boldsymbol{p}^b_{e_b}) \boldsymbol{T}(\boldsymbol{\phi}_b) \dot{\boldsymbol{\phi}}_b + \boldsymbol{R}_b \dot{\boldsymbol{p}}^b_{e_b}, \tag{5}$$
$$\dot{\boldsymbol{\phi}}_e = \boldsymbol{T}^{-1}(\boldsymbol{\phi}_e) \Big[\boldsymbol{T}(\boldsymbol{\phi}_b) \dot{\boldsymbol{\phi}}_b + \boldsymbol{R}_b \boldsymbol{T}(\boldsymbol{\phi}^b_e) \dot{\boldsymbol{\phi}}^b_e \Big], \tag{6}$$

where $\boldsymbol{\phi}_b$ and $\boldsymbol{\phi}^b_e$ are the RPY angles extracted form $\boldsymbol{R}_b$ and $\boldsymbol{R}^b_e$, respectively.

By defining $\boldsymbol{q}$ as the $(n \times 1)$ vector of manipulator joint positions, the velocities $\dot{\boldsymbol{p}}^b_{e_b}$ and $\boldsymbol{\omega}^b_e$ can be expressed in terms of the joint velocities $\dot{\boldsymbol{q}}$, via the manipulator Jacobian $\boldsymbol{J}^b_{e_b}$, as

$$\begin{bmatrix} \dot{\boldsymbol{p}}^b_{e_b} \\ \boldsymbol{\omega}^b_e \end{bmatrix} = \begin{bmatrix} \dot{\boldsymbol{p}}^b_{e_b} \\ \boldsymbol{T}(\boldsymbol{\phi}^b_e) \dot{\boldsymbol{\phi}}^b_e \end{bmatrix} = \boldsymbol{J}^b_{e_b} \dot{\boldsymbol{q}}. \tag{7}$$

By virtue of (7), the differential kinematics (5)-(6) can be rearranged in compact form as

$$\dot{\boldsymbol{x}}_e = \boldsymbol{J}_b(\boldsymbol{q}, \boldsymbol{\phi}_b) \dot{\boldsymbol{x}}_b + \boldsymbol{T}_A^{-1}(\boldsymbol{\phi}_e) \boldsymbol{J}_{e_b}(\boldsymbol{q}, \boldsymbol{\phi}_b) \dot{\boldsymbol{q}}, \tag{8}$$

where $\dot{\boldsymbol{x}}_b = \begin{bmatrix} \dot{\boldsymbol{p}}_b^{\mathrm{T}} & \dot{\boldsymbol{\phi}}_b^{\mathrm{T}} \end{bmatrix}^{\mathrm{T}}$, $\dot{\boldsymbol{x}}_e = \begin{bmatrix} \dot{\boldsymbol{p}}_e^{\mathrm{T}} & \dot{\boldsymbol{\phi}}_e^{\mathrm{T}} \end{bmatrix}^{\mathrm{T}}$,

$$\boldsymbol{T}_A(\boldsymbol{\phi}_e) = \begin{bmatrix} \boldsymbol{I}_3 & \boldsymbol{O}_3 \\ \boldsymbol{O}_3 & \boldsymbol{T}(\boldsymbol{\phi}_e) \end{bmatrix}, \quad \boldsymbol{J}_{e_b} = \begin{bmatrix} \boldsymbol{R}_b & \boldsymbol{O}_3 \\ \boldsymbol{O}_3 & \boldsymbol{R}_b \end{bmatrix} \boldsymbol{J}^b_{e_b}$$

and

$$\boldsymbol{J}_b = \begin{bmatrix} \boldsymbol{I}_3 & -\boldsymbol{S}(\boldsymbol{R}_b \boldsymbol{p}^b_{e_b}) \boldsymbol{T}(\boldsymbol{\phi}_b) \\ \boldsymbol{O}_3 & \boldsymbol{T}^{-1}(\boldsymbol{\phi}_e) \boldsymbol{T}(\boldsymbol{\phi}) \end{bmatrix},$$

where $\boldsymbol{I}_3$ and $\boldsymbol{O}_3$ denote, respectively, the (3×3) identity and null matrices.

Since, the quadrotor vehicle is an under-actuated system, namely it has only 4 independent control inputs and 6 DoFs, usually the position $\boldsymbol{p}_b$, and the yaw angle ψ_b are used as controlled variables, while roll and pitch angles, φ_b and θ_b, are used as intermediate control inputs for position control [17]. Hence, by grouping the motion variable as

$$\boldsymbol{\zeta} = \begin{bmatrix} \boldsymbol{p}_b \\ \psi_b \\ \boldsymbol{q} \end{bmatrix}, \quad \boldsymbol{\sigma} = \begin{bmatrix} \varphi_b \\ \theta_b \end{bmatrix},$$

the differential kinematics (8) can be rewritten in more compact form as

$$\dot{\boldsymbol{x}}_e = \boldsymbol{J}_\zeta(\boldsymbol{\sigma}, \boldsymbol{\zeta}) \dot{\boldsymbol{\zeta}} + \boldsymbol{J}_\sigma(\boldsymbol{\sigma}, \boldsymbol{\zeta}) \dot{\boldsymbol{\sigma}}, \tag{9}$$

where $\boldsymbol{J}_\zeta$ is composed by the columns of $\boldsymbol{J}_b$ corresponding to controlled variables and by $\boldsymbol{T}_A^{-1}(\boldsymbol{\phi}_e) \boldsymbol{J}_{e_b}$, while $\boldsymbol{J}_\sigma$ is composed by the remaining columns of $\boldsymbol{J}_b$.

Preprint version of the paper: E. Cataldi, G. Muscio, M.A. Trujillo, Y. Rodriguez, F. Pierri, G. Antonelli, F. Caccavale, A. Viguria, S. Chiaverini, A. Ollero, "Impedance control of an aerial-manipulator: Preliminary results" IEEE/RSJ International Conference on Intelligent Robots and Systems, pp. 3848-3853, 2016. DOI:10.1109/IROS.2016.7759566

B. Dynamics

The dynamic model of the aerial robotic manipulator, in the presence of environment interaction, by assuming negligible aerodynamic effects, can be expressed as

$$\boldsymbol{M}(\boldsymbol{\xi})\ddot{\boldsymbol{\xi}} + \boldsymbol{C}(\boldsymbol{\xi},\dot{\boldsymbol{\xi}})\dot{\boldsymbol{\xi}} + \boldsymbol{g}(\boldsymbol{\xi}) = \boldsymbol{u} + \boldsymbol{u}_e(\boldsymbol{h})\,, \tag{10}$$

where $\boldsymbol{\xi} = [\boldsymbol{x}_b^{\mathrm{T}} \quad \boldsymbol{q}^{\mathrm{T}}]^{\mathrm{T}} \in \mathbb{R}^{(6+n\times 1)}$, $\boldsymbol{M} \in \mathbb{R}^{(6+n\times 6+n)}$ is the symmetric and positive definite inertia matrix, $\boldsymbol{C} \in \mathbb{R}^{(6+n\times 6+n)}$ is the matrix of Coriolis and centrifugal terms, $\boldsymbol{g} \in \mathbb{R}^{(6+n\times 1)}$ is the vector of gravity generalized forces, $\boldsymbol{u}_e$ is the effect of the interaction generalized forces on the system, given by

$$\boldsymbol{u}_e = \begin{bmatrix} \boldsymbol{u}_{e,f} \\ \boldsymbol{u}_{e,\mu} \\ \boldsymbol{u}_{e,\tau} \end{bmatrix} = \begin{bmatrix} \boldsymbol{I}_3 & \boldsymbol{O}_3 \\ \boldsymbol{T}^{\mathrm{T}}(\boldsymbol{\phi}_b)\boldsymbol{S}(\boldsymbol{p}_{e_b}^b) & \boldsymbol{T}^{\mathrm{T}}(\boldsymbol{\phi}_b) \\ \multicolumn{2}{c}{\boldsymbol{J}_{e_b}^{\mathrm{T}}} \end{bmatrix} \boldsymbol{h}, \tag{11}$$

where $\boldsymbol{h} = \begin{bmatrix} \boldsymbol{h}_f & \boldsymbol{h}_\mu \end{bmatrix}^{\mathrm{T}}$ is the vector stacking the forces ($\boldsymbol{h}_f$) and moments ($\boldsymbol{h}_\mu$) exerted on the manipulator end-effector. Finally, $\boldsymbol{u}$ is the vector of control inputs,

$$\boldsymbol{u} = \begin{bmatrix} \boldsymbol{u}_f \\ \boldsymbol{u}_\mu \\ \boldsymbol{u}_\tau \end{bmatrix} = \begin{bmatrix} \boldsymbol{R}_b(\boldsymbol{\phi}_b)\boldsymbol{f}_b^b \\ \boldsymbol{T}^{\mathrm{T}}(\boldsymbol{\phi}_b)\boldsymbol{R}_b(\boldsymbol{\phi}_b)\boldsymbol{\mu}_b^b \\ \boldsymbol{\tau} \end{bmatrix}, \tag{12}$$

where $\boldsymbol{\tau}$ is the $(n\times 1)$ vector of the manipulator joint torques, $\boldsymbol{f}_b^b$ and $\boldsymbol{\mu}_b^b$ are the (3×1) vectors of the forces and the moments generated by the 4 rotors of the quadrotor vehicle, expressed in the frame Σ_b.

III. Control Architecture

When the end-effector of the aerial manipulator interacts with the external environment, for example during the grasping/deployment of an object or in the case of an unexpected collision, the end-effector experiences raising forces in the direction of the interaction; in order to ensure bounded interaction forces, it could be worth ensuring a compliant behavior of the system. This goal can be achieved by resorting to the impedance control paradigm [10].

The proposed control architecture, depicted in Fig. 3, is composed by 3 modules:

- Impedance module: it receives, as input, the desired end-effector trajectory from the off-line planner and computes the reference motion, on the basis of the sensed forces (measured by the wrist force/torque sensor), in order to make the system behave like a mechanical impedance.
- Inverse kinematic module, which, based on the trajectory coming from the previous module, computes the reference value of the motion variables $\boldsymbol{\zeta}$, through a Closed Loop Inverse Kinematic (CLIK) algorithm [16]. At this level, the system redundancy is handled in a prioritized way via the Null Space based Behavioral control approach [18].
- Motion controller: it ensures the tracking of the reference values output by the impedance module.

A. Impedance module

In order to achieve bounded interaction forces, a compliant behavior of the end-effectors is enforced. To this aim, an impedance module is suitably designed in order to make the end-effector of the aerial manipulator behave like a mass–spring-damper system, i.e., a mechanical impedance. The desired trajectory for the end-effector, $\mathcal{T}_d = \{\boldsymbol{x}_{e,d}, \dot{\boldsymbol{x}}_{e,d}, \ddot{\boldsymbol{x}}_{e,d}\}$, computed via off-line planner is fed to the impedance filter. In detail, the reference trajectory, $\mathcal{T}_r = \{\boldsymbol{x}_{e,r}, \dot{\boldsymbol{x}}_{e,r}, \ddot{\boldsymbol{x}}_{e,r}\}$, is obtained by integrating the following second order differential equation

$$\boldsymbol{M}_e\Delta\ddot{\boldsymbol{x}}_e + \boldsymbol{D}_e\Delta\dot{\boldsymbol{x}}_e + \boldsymbol{K}_e\Delta\boldsymbol{x}_e = \boldsymbol{\gamma}, \tag{13}$$

where $\Delta\boldsymbol{x}_e = \boldsymbol{x}_{e,d} - \boldsymbol{x}_{e,r}$, $\boldsymbol{\gamma} = \boldsymbol{T}_A^{\mathrm{T}}(\boldsymbol{\phi}_e)\boldsymbol{h}$, while $\boldsymbol{M}_e$, $\boldsymbol{D}_e$ and $\boldsymbol{K}_e$ are positive definite (6×6) matrices representing the mass, damping and stiffness of the desired impedance.

B. Inverse kinematic module

Once the reference trajectory of the end-effector is known, a Closed Loop Inverse Kinematics algorithm computes the reference motions for the controlled variables [19]. It is worth remarking that an aerial manipulator has $4+n$ actuated DOFs while a task, in the Cartesian space, could require at most 6 DOFs, thus aerial manipulators are often kinematically redundant systems. By recalling the differential kinematics (9), and considering a redundant aerial manipulator, the time derivative of the commanded controlled variables, $\dot{\boldsymbol{\zeta}}_c$, can be expressed as follows

$$\begin{aligned} \dot{\boldsymbol{\zeta}}_c \;=\; & \boldsymbol{J}_\zeta^\dagger(\boldsymbol{\sigma},\boldsymbol{\zeta}_c)\left(\dot{\boldsymbol{x}}_{e,r} + \boldsymbol{K}\boldsymbol{e}\right) - \\ & \boldsymbol{J}_\zeta^\dagger(\boldsymbol{\sigma},\boldsymbol{\zeta}_c)\boldsymbol{J}_\sigma(\boldsymbol{\sigma},\boldsymbol{\zeta}_c)\dot{\boldsymbol{\sigma}} + \boldsymbol{N}_{J_\zeta}\dot{\boldsymbol{q}}_0\,, \end{aligned} \tag{14}$$

where $\boldsymbol{J}_\zeta^\dagger = \boldsymbol{W}^{-1}\boldsymbol{J}_\zeta^{\mathrm{T}}\left(\boldsymbol{J}_\zeta\boldsymbol{W}^{-1}\boldsymbol{J}_\zeta^{\mathrm{T}}\right)^{-1}$ is a weighted pseudoinverse of $\boldsymbol{J}_\zeta$, with $\boldsymbol{W}$ a positive definite weight matrix, that allows to relatively weight the vehicle and joint velocities. $\boldsymbol{K}$ is a symmetric positive definite gain matrix, $\boldsymbol{e} = \boldsymbol{x}_{e,r} - \boldsymbol{x}_{e,c}$ is the kinematic inversion error, $\boldsymbol{x}_{e,c}$ is the end-effector pose computed on the basis of $\boldsymbol{\zeta}_c$ and the measured roll and pitch angles, $\boldsymbol{\sigma}$, through the direct kinematics. The other terms in (14) are: $\boldsymbol{N}_{J_\zeta} = \boldsymbol{I}_{4+n} - \boldsymbol{J}_\zeta^\dagger\boldsymbol{J}_\zeta$ is a projector onto the null space of $\boldsymbol{J}_\zeta$ and $\dot{\boldsymbol{q}}_0$ is a vector of joint velocities corresponding to internal motions, i.e. joint motions which do not affect the end-effector configuration. Such internal motions can be exploited to fulfill secondary tasks, by resorting to task-priority algorithms such as the Null Space based Behavioral control [18].

C. Motion controller

Since the motion references for the controlled variables, $\boldsymbol{\zeta}_c$, have been computed by the Inverse kinematics module, a motion controller has to be designed in order to ensure motion tracking. The described impedance control scheme is, in principle, compatible with any motion controller; in this section, the control algorithm for an aerial manipulator system equipped with a 6-DOFs arm, developed within the ARCAS project, is presented. Since the weight of the 6-DOFs arm is significant with respect to the total platform

Preprint version of the paper: E. Cataldi, G. Muscio, M.A. Trujillo, Y. Rodriguez, F. Pierri, G. Antonelli, F. Caccavale, A. Viguria, S. Chiaverini, A. Ollero, "Impedance control of an aerial-manipulator: Preliminary results" IEEE/RSJ International Conference on Intelligent Robots and Systems, pp. 3848-3853, 2016. DOI:10.1109/IROS.2016.7759566

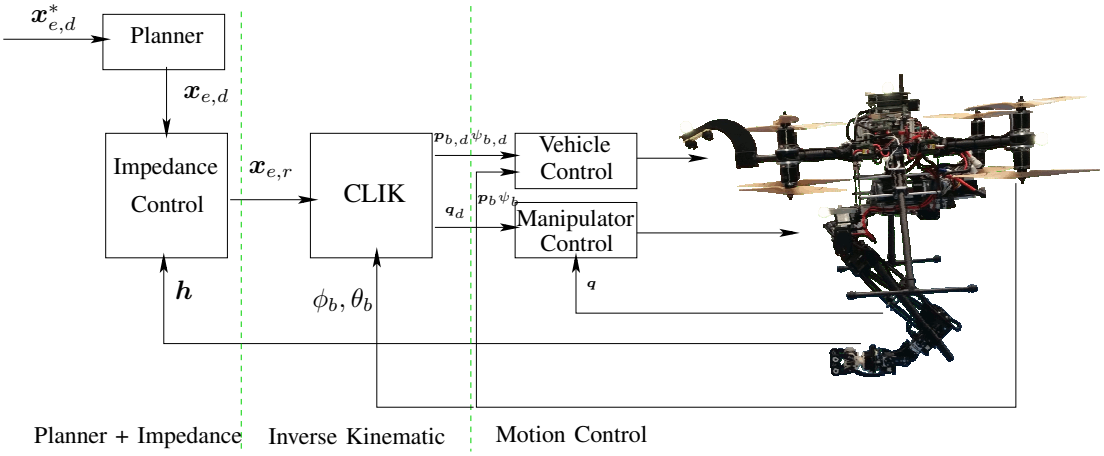

Fig. 3. Sketch of the control loop.

mass, a special control architecture, based on a moving tray in charge of moving the batteries in order to compensate the center of mass displacements, allows to keep the aerial platform stable when the arm is moving.

The ARCAS motion controller architecture is composed by 4 main modules: one of them is specifically added for the robotic arm control while the others are standard modules for multirotor control, even-though they have been suitably modified for the existing setup. In detail:

- The Estimator and Data Processing Module estimates and processes the state of the aerial manipulator (position, attitude, angular velocity, servos data, sensors and safety operator radio references).
- The Position Controller Module ensures platform stabilization in the 3D space; position references represent the input for the attitude controller.
- The Attitude Controller module receives references from the position controller and stabilizes the platform commanding each motor. It also hosts a compensation module, with the goal of rejecting the perturbations due to the arm movement.
- The Robotic Arm Controller module is in charge of tracking the references computed for the arm joints, as well as, its deployment and retraction.

For the sake of brevity, the motion controller is not detailed here, the interested reader is referred to [20].

IV. Experimental results

In order to test the effectiveness of the proposed control scheme two experimental case studies have been performed on the ARCAS setup, composed of an aerial multi-rotor platform equipped with a 6-DOFs manipulator, designed and manufactured by CATEC. The first two modules of the proposed control, namely the Impedance and Inverse kinematics modules, have been developed in C++ under ROS (Robot Operating System) environment [21] and were running on the i7 Asctec Mastermind onboard computer, while the motion controller, described in Secion III-C, was running on the autopilot. As concerns the sensor data feedback, for the vehicle position the VICON system [22] has been used, the vehicle attitude is provided by the IMU, joint position are directly provided by the servos, while a force/torque sensor mounted on the manipulator wrist gives force feedback data (control and sensing frequencies are collected in Table I).

Control		Sensor	
Impedance	100 Hz	Force	100 Hz
Clik	100 Hz	Position	100 Hz
Quadrotor Attitude	100 Hz	Orientation	100 Hz
Quadrotor Position	100 Hz	Joint	50 Hz
Manipulator	50 Hz		

TABLE I
CONTROL AND SENSING FREQUENCIES.

	Position			Orientation		
	Impedence control					
M_e	1	1	1	1	1	1
D_e	35	35	35	2	2	2
K_e	25	25	25	1	1	1
	CLIK					
k	10	10	10	10	10	10

TABLE II
THE CONTROL GAINS.

In the Table II the control gains are reported.

Two different experiments have been considered, in which the external interaction has been obtained via different materials. More in detail, in the first experiment a rope has been used, see Fig. 1 (left), i.e., one end of the rope has been blocked on the end-effector and the other one has been pulled by a human operator. In the second experiment, a semi-flexible bar has been used in lieu of the rope, see Fig. 1 (right).

The kinematic inversion (14) has been performed by adopting the following weight matrix, $\boldsymbol{W}$

$$\boldsymbol{W} = \mathrm{diag}\left[100\boldsymbol{I}_4\,, \boldsymbol{I}_6\right],$$

in such a way to weigh the joint velocities more than the vehicle's ones. In other words, the behavior of the

Preprint version of the paper: E. Cataldi, G. Muscio, M.A. Trujillo, Y. Rodriguez, F. Pierri, G. Antonelli, F. Caccavale, A. Viguria, S. Chiaverini, A. Ollero, "Impedance control of an aerial-manipulator: Preliminary results" IEEE/RSJ International Conference on Intelligent Robots and Systems, pp. 3848-3853, 2016. DOI:10.1109/IROS.2016.7759566

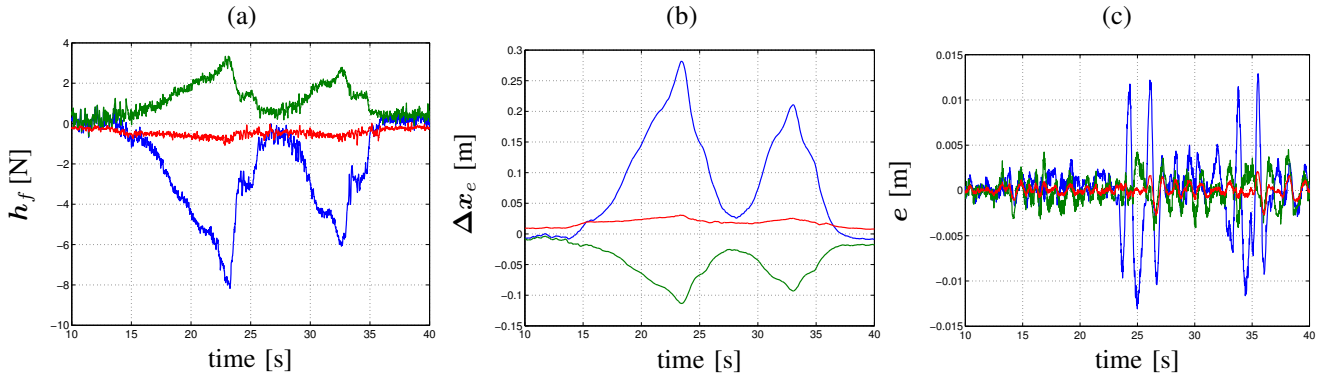

Fig. 4. *Rope experiment* – (a) Force sensed by the manipulator wrist.(b) Time line of the impedance error. (c) The inverse kinematics error. Where the x-axes (blue), y-axes (green) and z-axes (red).

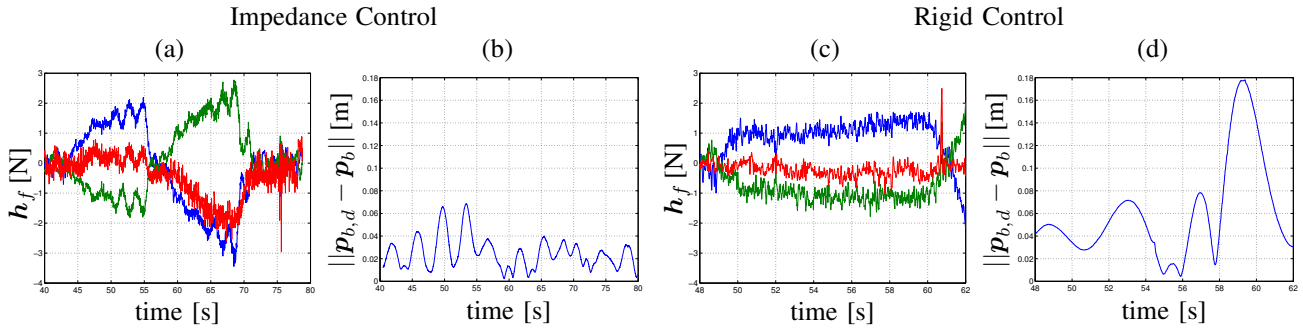

Fig. 5. *Semi-flexible bar experiment* – (a-c) The forces sensed on the manipulator wrist for the impedance control (a) and the rigid control (c), x-axes (blue), y-axes (green) and z-axes (red).(b-d) Norm of the vehicle position error the impedance control (b), and the rigid control (d).

manipulator joints has been designed to be more compliant with respect to the UAV behavior.

The forces measured by the force/torque sensor have been previously calibrated and expressed in terms of inertial frame coordinates.

A. Experiment with the rope

Figure 4 illustrates the experimental results when the end-effector is pulled/pushed by a rope.

In detail, Fig. 4.a shows the forces exerted on the manipulator wrist: as can be viewed the rope has been pulled and released twice, with a maximum force magnitude of about 8.8 N. The maximum interaction forces are experienced along the x, y axes as it can be recognized from Fig. 1 (left).

According to the forces exerted, the impedance errors, namely $\Delta x_e = \boldsymbol{x}_{e,d} - \boldsymbol{x}_{e,r}$, shown in Fig. 4.b, are larger along the directions where the forces are larger as well. In other words, the impedance errors represent a measure of the end-effector compliance.

Figure 4.c shows the time history of the position kinematic inversion error, i.e., the difference between the reference output by the impedance module and the end-effector position computed on the bases of the commanded control variable, $\boldsymbol{\zeta}_c$.

B. Experiment with the Semi-flexible Bar

In order to increase the rigidity of the external environment, the system has been solicited through a semi-flexible bar. To highlight the performance of the proposed control approach a comparison with a rigid controller, namely without force feedback, is presented, in detail the benchmark control is structured as the control proposed in Figure 3, without the impedance control block.

Figure 5.a-c shows the measured forces, in the case the impedance control is active (a) and in the case of rigid control (c). As it can be appreciated, the interactions generated on the end-effector during the two experiments are not the same, since, as can be easily understood, it is not possible replicate exactly the same interaction twice.

When the impedance control is not active, even though the measured forces are lower than those experienced when the impedance control is running, the system is driven to instability. This effect can be appreciated in the video available at the link `www.elisabettacataldi.it/video/InteractionSevilleGood.webm`

To highlight the difference, in terms of performance, between the proposed control and its benchmark, it can analyzed the norm of the vehicle position error shown in Fig. 5.b-d: in detail, on Fig. 5.b there is the result in the case of impedance control while on Fig. 5.d the result in presence of the rigid one. By recalling that, thanks to the weight matrix, the compliant behavior is superimposed only to the manipulator, while the vehicle is attended to be almost rigid with respect to the external interaction, the norm of the vehicle position error remains below a maximum value of about 6.8 cm. In other words, the effect of the interaction

Preprint version of the paper: E. Cataldi, G. Muscio, M.A. Trujillo, Y. Rodriguez, F. Pierri, G. Antonelli, F. Caccavale, A. Viguria, S. Chiaverini, A. Ollero, "Impedance control of an aerial-manipulator: Preliminary results" IEEE/RSJ International Conference on Intelligent Robots and Systems, pp. 3848-3853, 2016. DOI:10.1109/IROS.2016.7759566

forces are adsorbed by the manipulator: it is a desirable behavior, since the aerial platform is under actuated, and, thus, not able to directly counteract the forces lying on the rotor plane by modifying the roll and/or pitch angles. Therefore, it is worth ensuring that the interaction forces acting on the platform base are as low as possible. On the other hand, when the impedance is not active, the forces transmitted to the aerial platform are larger and cause a larger position error, with a peak value of about 18 cm.

The impedance error is shown in Fig. 6.a, as for the rope case, this figure shows how the impedance control counteracts the rigidity of the system making the manipulator compliant.

Figure 6.b shows the inverse kinematics error, from which it can be appreciated that the algorithm works properly also in the presence of interaction with a more rigid environment.

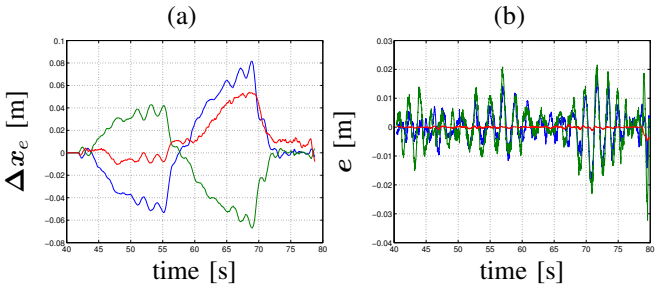

Fig. 6. *Semi-flexible bar experiment* – (a) Time line of the impedance error. (b) The inverse kinematics error, x-axes (blue). Wherer y-axes (green) and z-axes (red).

V. Conclusion

In this paper an impedance control for aerial robotic manipulators has been presented, the proposed control is composed by 3 modules: an impedance filter, an inverse kinematic module and a motion controller.

Such a controller is a preliminary step towards the cooperative transportation of an object accomplished by a team of aerial robotic manipulators. The main goal is to avoid excessive mechanical stresses on the grasped object and, at the same time, to reduce the forces exerted on the manipulators and the aerial bases.

Acknowledgments

The research leading to these results has received funding from the European Commission's 7th Framework Program under grant agreement No.287617 (IP project ARCAS - Aerial Robotics Cooperative Assembly system) and from the European Commission's Horizon 2020 Program under grant agreement No. 644271 (IP project AEROARMS - AErial RObotic system integrating multiple ARMS and advanced manipulation capabilities for inspection and maintenance).

References

[1] D. Mellinger, Q. Lindsey, M. Shomin, and V. Kumar, "Design, modelling, estimation and control for aerial grasping and manipulation," in *Proc. of IEEE/RSJ International Conference on Intelligent Robots and Systems*, 2011, pp. 2668–2673.

[2] P. Pounds, D. Bersak, and A. Dollar, "Grasping from the air: Hovering capture and load stability," in *Proc. of IEEE Int. Conf. on Robotics and Automation (ICRA)*, 2011, pp. 2491–2498.

[3] M. Orsag, C. Korpela, and P. Oh, "Modeling and control of MM-UAV: Mobile manipulating unmanned aerial vehicle," *Journal of Intelligent and Robotic Systems*, vol. 69, pp. 227–240, 2013.

[4] F. Caccavale, G. Giglio, G. Muscio, and F. Pierri, "Adaptive control for uavs equipped with a robotic arm," in *Proc. of the 19th World Congress of the International Federation of Automatic Control (IFAC)*, 2014.

[5] K. Baizid, G. Giglio, F. Pierri, M. Trujillo, G. Antonelli, F. Caccavale, A. Viguria, S. Chiaverini, and A. Ollero, "Experiments on behavioral coordinated control of an unmanned aerial vehicle manipulator system," in *Robotics and Automation (ICRA), 2015 IEEE International Conference on*. IEEE, 2015, pp. 4680–4685.

[6] ——, "Behavioral control of unmanned aerial vehicle manipulator systems," *Autonomous Robots*, pp. 1–18, 2016.

[7] M. Orsag, C. Korpela, S. Bogdan, and P. Oh, "Valve turning using a dual-arm aerial manipulator," in *Unmanned Aircraft Systems (ICUAS), 2014 International Conference on*. IEEE, 2014, pp. 836–841.

[8] H. Tsukagoshi, M. Watanabe, T. Hamada, D. Ashlih, and R. Iizuka, "Aerial manipulator with perching and door-opening capability," in *Robotics and Automation (ICRA), 2015 IEEE International Conference on*, May 2015, pp. 4663–4668.

[9] S. Kim, H. Seo, and H. Kim, "Operating an unknown drawer using an aerial manipulator," in *Robotics and Automation (ICRA), 2015 IEEE International Conference on*, May 2015, pp. 5503–5508.

[10] N. Hogan, "Impedance control: An approach to manipulation: Parts i-iii," *Journal of dynamic systems, measurement, and control*, vol. 107, no. 1, pp. 1–24, 1985.

[11] V. Lippiello and F. Ruggiero, "Cartesian impedance control of uav with a robotic arm," in *Proc. of 10th International IFAC Symposium on Robot Control (SYROCO)*, 2012, pp. 704–709.

[12] G. Giglio and F. Pierri, "Selective compliance control for an unmanned aerial vehicle with a robotic arm," in *22nd Mediterranean Conference of Control and Automation (MED)*. IEEE, 2014, pp. 1190–1195.

[13] F. Caccavale, G. Giglio, G. Muscio, and F. Pierri, "Cooperative impedance control for multiple UAVs with a robotic arm," in *2015 IEEE/RSJ International Conference on Intelligent Robots and Systems (IROS)*, 2015, pp. 2366–2371.

[14] F. Forte, R. Naldi, A. Macchelli, and L. Marconi, "Impedance control of an aerial manipulator," in *American Control Conference (ACC), 2012*. IEEE, 2012, pp. 3839–3844.

[15] "ARCAS - Aerial Robotics Cooperative Assembly System," 20/10/2013. [Online]. Available: http://www.arcas-project.eu

[16] B. Siciliano, L. Sciavicco, L. Villani, and G. Oriolo, *Robotics: modelling, planning and control*. Springer Verlag, 2009.

[17] G. Antonelli and E. Cataldi, "Adaptive control of arm-equipped quadrotors. theory and simulations," in *Control and Automation (MED), 2014 22nd Mediterranean Conference of*, June 2014, pp. 1446–1451.

[18] G. Antonelli, F. Arrichiello, and S. Chiaverini, "The Null-Space-based Behavioral control for autonomous robotic systems," *Journal of Intelligent Service Robotics*, vol. 1, no. 1, pp. 27–39, Jan. 2008.

[19] G. Arleo, F. Caccavale, G. Muscio, and F. Pierri, "Control of quadrotor aerial vehicles equipped with a robotic arm," in *Proc. of 21th Mediterranean Conference on Control and Automation*, 2013, pp. 1174–1180.

[20] F. Ruggiero, M. Trujillo, R. Cano, H. Ascorbe, A. Viguria, C. Perez, V. Lippiello, A. Ollero, and B. Siciliano, "A multilayer control for multirotor UAVs equipped with a servo robot arm," in *IEEE Int. Conf. on Robotics and Automation (ICRA)*, 2015, pp. 4014–4020.

[21] M. Quigley, B. Gerkey, K. Conley, J. Faust, T. Foote, J. Leibs, E. Berger, R. Wheeler, and A. Ng., "Ros: an open-source robot operating system," in *Open-source software workshop of the 2009 IEEE International Conference on Robotics and Automation*, Kobe, J, 2009.

[22] VICON, "Vicon Motion Systems," Ltd. [Online]. Available: http://www.vicon.com

Preprint version of the paper: E. Cataldi, G. Muscio, M.A. Trujillo, Y. Rodriguez, F. Pierri, G. Antonelli, F. Caccavale, A. Viguria, S. Chiaverini, A. Ollero, "Impedance control of an aerial-manipulator: Preliminary results" IEEE/RSJ International Conference on Intelligent Robots and Systems, pp. 3848-3853, 2016. DOI:10.1109/IROS.2016.7759566